Monte Carlo study of electron transport in zincblende and wurtzite InN

M. AKARSU*, S. KARAKAYA, S. AYDOGU[a], O. OZBAS
Physics Department, Eskişehir Osmangazi University, Eskişehir, Turkey
[a]*Physics Department, Dumlupınar University, Kütahya, Turkey*

The influence of InN crystal symmetry (zincblende and wurtzite) on low-field and high-field electron transport is studied by the Monte Carlo method. Calculations are made using a nonparabolic effective mass energy band model. Ionized impurity, acoustic phonon, polar optical phonon, intervalley and dislocation scattering are included in the simulation. It is found that at a field of 35 kV/cm that the peak electron drift velocity is 4.2×10^7 cm/s for the zincblende InN. The peak velocity is about 20% higher in wurtzite InN (5.1×10^7 versus 4.2×10^7 cm/s) and reaches at a field of 25 kV/cm.

(Received January 31, 2011; accepted May 31, 2011)

Keywords: Monte Carlo, Electron transport, Dislocation scattering, İndium nitride

1. Introduction

The discovery of the low band gap of InN has led to intensive studies of the electronic properties of this material. Owing to the low band gap within this material, InN offers some important advantages in the fabrication of high-frequency transistors operating at high powers and temperatures due to its potentially superior performance over other III-nitrides [1-5]. The vast majority of research on InN has been focused on the wurtzite (WZ) crystal phase [6-8]. The reason is that most InN has been grown on sapphire substrates which generally transfer their hexagonal symmetry to the InN film. Nevertheless, zincblende (ZB) InN layers have been grown and the electronic structure of this InN phase has been calculated recently [9-12]. In this paper, we present calculations of the electronic transport properties in both phases of InN. Results of the simulations in bulk material, such as drift velocity, average electron energy, central valley occupancy and low-field electron mobility are presented and the difference between the transport properties of two phases is discussed.

2. Model description

The Monte Carlo method has been widely used to study electron transport in semiconductors. It provides a useful tool for the development, analysis and understanding of semiconductor devices [13-18]. The Monte Carlo method, as applied to charge transport in semiconductors, consist of a simulation of the motion of electron inside the crystal, subject to the action of external forces due to applied electric field and of given scattering mechanisms. The principal input for the Monte Carlo method used in the transport calculations is the band structure description of the semiconductor material. A nonparabolic three-valley model for the conduction band is employed both ZB and WZ crystal phases of bulk indium nitride. The nanparabolicity being treated through the application of the following form:

$$\frac{\hbar^2 k^2}{2m^*} = \gamma(E) = E(1 + \alpha E) \qquad (1)$$

$$\alpha = \frac{1}{E_g}\left(1 - \frac{m^*}{m_0}\right)^2 \qquad (2)$$

Where $\hbar$ is the reduced Planck constant, k is the wave vector, E is the electron energy relative to the bottom of valleys, m^* is the effective mass at the band edge, m_0 is free electron mass and E_g is the energy gap of semiconductor. The band parameters for the valleys given in Table 1 are extracted from recent band structure calculations [19,20]. Material parameters necessary for calculating the scattering probabilities used in the Monte Carlo simulations are tabulated in Table 2 [21-23]. Due to the uncertainty in the values, the material parameters of ZB InN are taken identical to those of WZ InN.

Table 1. Band structure parameters of InN.

ZB InN	Conduction band valley	Γ	X	K	Ref.
	Intervalley separation (eV)	0.0	3.2	4.71	[19]
	Effective mass (m^*/m_0)	0.054	0.67	0.53	[19]
	Energy gap (eV)	0.53			[20]
WZ InN	Conduction band valley	Γ_1	Γ_3	M-L	
	Intervalley separation (eV)	0.0	1.78	2.71	[19]
	Effective mass (m^*/m_0)	0.04	0.25	1.0	[19]
	Energy gap (eV)	0.7			[20]

Table 2. Material parameters of ZB and WZ InN.

Parameter	Value	Ref.
Mass density (g/cm^3)	6.81	[21]
Longitudinal sound velocity (cm/s)	6.24x10^5	[21]
Transverse sound velocity (cm/s)	2.55x10^5	[21]
Static dielectric constant ($\varepsilon_s/\varepsilon_0$)	15.3	[22]
High-frequency dielectric constant ($\varepsilon_\infty/\varepsilon_0$)	8.4	[22]
Intervalley deformation potential (eV/cm)	1x10^9	[23]
Acoustic deformation potential (eV)	7.1	[23]
Optical phonon energy (meV)	89	[23]
Intervalley optical phonon energy (meV)	73	[23]

Scattering mechanisms considered are ionized impurity, polar optical phonon, acoustic deformation potential, intervalley and dislocation scattering.

Using the relation $\mu = v_d/E$, low-field mobility is obtained from a straight line of the velocity-electric field curve at low electric field strength. Electron transport is studied using the single particle Monte Carlo method in the simulation time of 2 ns.

3. Results and discussion

Fig. 1 show the electron drift velocity in both ZB and WZ InN calculated as a function of the applied electric field with and without dislocations for a crystal temperature of 300 K, assuming free electron and ionized impurity concentrations of 10^{17} cm^{-3}. The difference in the calculated drift velocities between the two crystal phases is obvious.

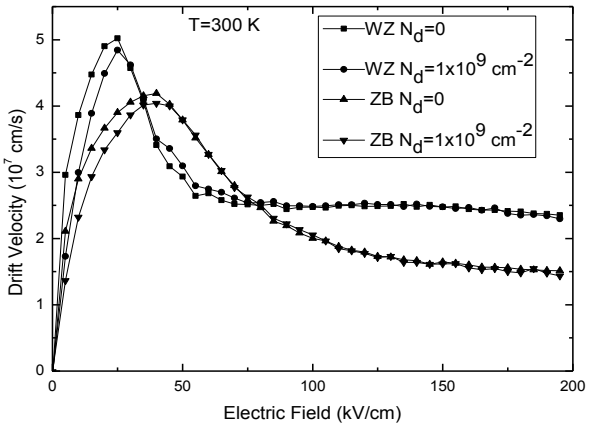

Fig. 1. Electron drift velocity as a function of the applied electric field for ZB and WZ InN at 300 K and with the dislocation concentrations of 1×10^9 cm^{-2}.

While in the case of WZ InN, the velocity increases with increasing electric field more rapidly owing to the lower effective mass in the central valley, the velocity increase in the case of ZB InN is relatively slower. In low electric field strengths, influence of the dislocation scattering is significant; dislocations reduce the drift velocity in both materials. However, with increasing electric field strength, the effects of dislocations decrease, as intervalley and polar optical phonon scattering play more important roles on the drift velocity. It is found that at a field of 25 kV/cm that the peak electron drift velocity is 5.1×10^7 cm/s for the WZ InN. The peak velocity is about 20% lower in ZB InN (5.1×10^7 versus 4.2×10^7 cm/s) and reaches at a field of 35 kV/cm. Any further increase of the electric field strength results in reduced drift velocity for both materials and a region of negative differential resistance are observed. It is due to the transfer of electrons from the central valley, where they have small effective mass, to the upper valleys, where they have a larger effective mass. Fig. 2 shows the electric field dependence of the average electron energy. At the electric field strength in the range of 0-25 kV/cm, electrons are located in low energy central valley as shown in Fig. 3. When the electric field is in the range of 25-50 kV/cm, a rapid transfer from the central Γ_1 valley to the Γ_3 valley occurs, and the occupation of the Γ_3 valleys increases, and results in a sharp increase in average energy in this field region. However, when the electric field increases to 50-200 kV/cm, the electrons are almost set on the Γ_3 valleys and undergo a very frequent intervalley scattering. At this moment, for a large mass and high energy, the electron is difficult to accelerate. As a result, the velocity of electron no longer changes with the applied electric field, which is the so-called velocity saturation.

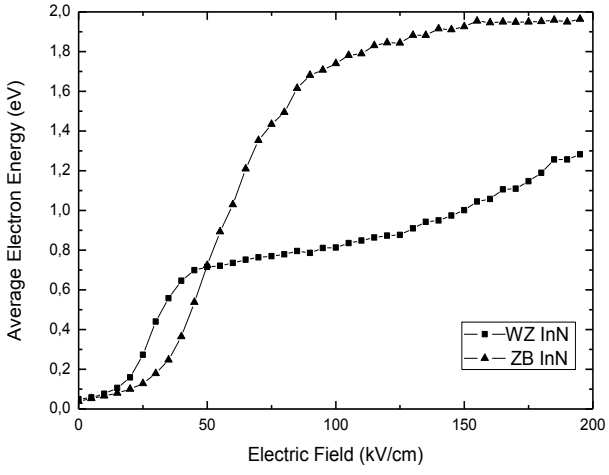

Fig. 2. Average electron energy as a function of the applied electric field for ZB and WZ InN.

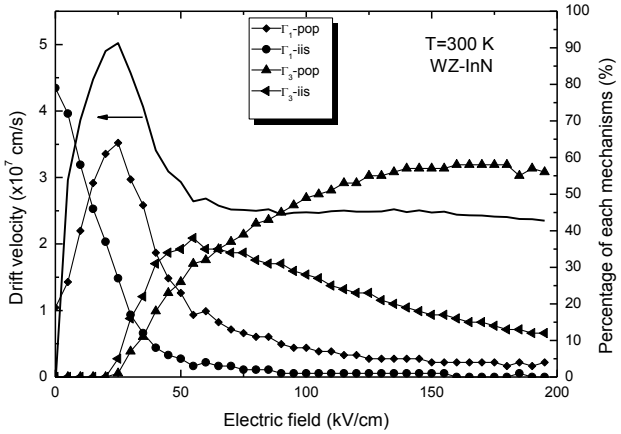

Fig. 3. Drift velocity and percentage of each scattering mechanisms in the central (Γ_1) and satellite (Γ_3) valleys as a function of the applied electric field for WZ InN. Pop is due to the polar optical phonon, iss is due to the ionized impurity scattering.

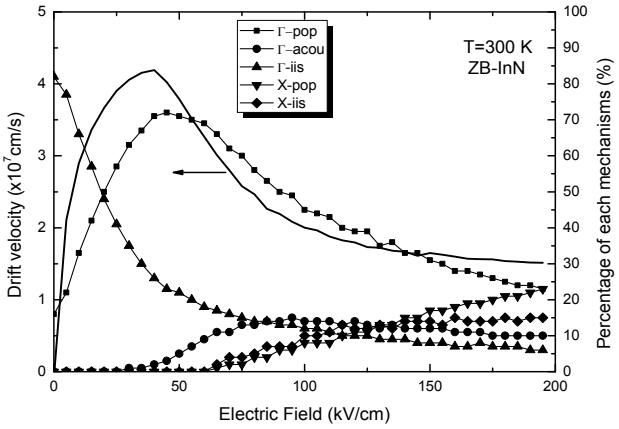

Fig. 5. Drift velocity and percentage of each scattering mechanisms in the central (Γ) and satellite (X) valleys as a function of the applied electric field for ZB InN. Pop is due to the polar optical phonon, acou is due to the acoustic phonon, iss is due to the ionized impurity scattering.

Fig. 4 and Fig. 5 shows the electron drift velocities and percentage of each scattering mechanisms as a function of applied electric field for WZ and ZB InN respectively. As shown in Fig. 4 and Fig. 5 for the low electric field values, ionized impurity scattering decrease rapidly with the increasing electric field strength while polar optical phonon scattering increase rapidly in both materials. An important difference between the two materials is the value of threshold field. The threshold fields are determined to be 25 kV/cm for the WZ and 50 kV/cm for the ZB phases, respectively. The reason is the large separation between the central and satellite valleys of 3.2 eV.

The effect of structural defects on the low-field electron mobility in bulk ZB and WZ InN at 300 K is shown in Fig. 6 as a function of the dislocation density. There is a significant dislocation effect on the low field mobility because the scattering of the dislocations significantly influences the low-field drift velocity. In Fig. 6, as the dislocation density exceeds ND=108 cm^{-2}, the low-field mobility starts to decrease for the both material phases. In the range of ND=108-1011 cm^{-2}, roomtemperature mobility is strongly dependent on the dislocation density with a decrease 2400 cm^2/Vs at 108 cm^{-2} to 500 cm^2/Vs at 1011 cm^{-2} for the WZ InN and 1800 cm^2/Vs at 108 cm^{-2} to 500 cm^2/Vs for the ZB InN respectively.

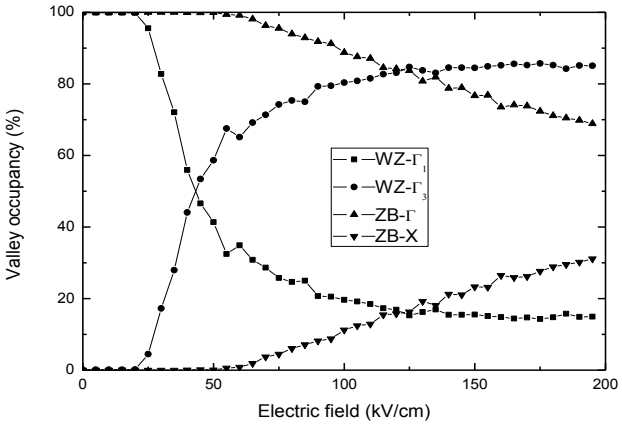

Fig. 4. Valley occupancies as a function of the applied electric field for ZB and WZ InN.

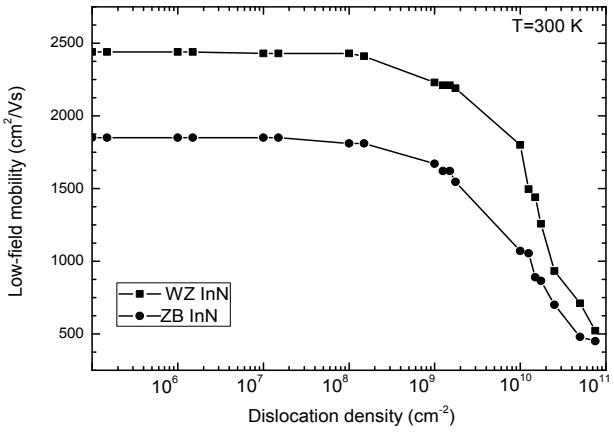

Fig. 6. Low-field electron mobility in ZB and WZ InN calculated at room temperature as a function of dislocation concentrations.

4. Conclusions

Results of the Monte Carlo simulations of the electron transport in both ZB and WZ phases of indium nitride have been presented. The dependencies of the drift velocity, average electron energy, valley occupancies on the electric field are shown and the effect of dislocations on the low-field mobility is studied. It is found that at a field of 35 kV/cm that the peak electron drift velocity is 4.2×107 cm/s for the ZB InN. The peak velocity is found about 20% higher in WZ InN (5.1×107 versus 4.2×107 cm/s) and reached at a field of 25 kV/cm. A region of negative differential resistance is observed in both material phases and the values of the threshold field are found to be 25 kV/cm and 35 kV/cm for the WZ and ZB phases, respectively. The low-field electron mobility in both materials decreases drastically for ND=108-1011 cm^{-2} as the dislocation density increase at room temperature. For low dislocation density, the room temperature mobility does not depend on ND. Finally, we found that WZ InN has a high peak drift velocity, a large saturation drift velocity and high low-field mobility compared to ZB InN.

References

[1] S. K. O'Leary, B. E. Foutz, M. S. Shur, U. V. Bhapkar, J. Appl. Phys. **83**, 826 (1998).
[2] M. Farahmand, C. Garetto, E. Belotti, Kevin F. Brennan, Michele Goano, Enrico Ghillino, Giovanni Ghione, John D. Albrecht and P. Paul Ruden., IEEE Transaction on Electron Dev. **48**, 9383 (2001).
[3] A. F. M. Anwar, S. Wu, R. T. Webster, IEEE Transaction on Electron Dev. **48**, 567 (2001).
[4] V. M. Polyakov, F. Schewierz, D. Fritsch, H. Schimidt, Phys. Stat. Sol. **3**, 598 (2006).
[5] C. Bulutay, B. K. Ridley, Superlattices and Microstructures **36**, 465 (2004).
[6] B. E. Foutz, S. K. O'Leary, M. S. Shur, L. F. Eastman, J. Appl. Phys. **85**, 7727 (1999).
[7] L. Hsu, R. E. Jones, S. X. Liu, K. M. Yu, W. Walukiewicz, J. Appl. Phys. **102**, 073705 (2007).
[8] V. M. Polyakov, F. Schewierz, J. Appl. Phys. **99**, 113705 (2006).
[9] J. Futhmüller, P. H. Hahn, F. Fuchs, F. Bechstedt, Phys. Rev. B **72**, 205106 (2005).
[10] D. Fritsch, H. Schmidt, M. Grundmann, Phys. Rev. B **69**, 165204 (2004).
[11] P. Carrier, S. Wei, J. Appl. Phys. **97**, 033707 (2005).
[12] N. Bouarissa, Eur. Phys. J. B **26**, 153 (2002).
[13] W. Walukiewicz, Physica E **20**, 300 (2004).
[14] E. Bellotti, B. K. Doshi, K. F. Brennan, J. D. Albrecht, P. Ruden, J. Appl. Phys. **85**, 916 (1999).
[15] S. K. O'Leary, B. E. Foutz, M. S. Shur, U. V. Bhapkar, Solid State Commun. **105**, 621 (1998).
[16] M. Akarsu, O. Ozbas, Math. Comput. Appl. **10**, 19 (2005).
[17] O. Ozbas, M. Akarsu, Turk J. Phys. **26**, 283 (2002).
[18] Xin-Gang Yu, Xin-Gang Liang, J. Appl. Phys. **103**, 043707 (2008).
[19] V. M. Polyakov, F. Schewierz, F. Fuchs, J. Futhmüller, Appl. Phys. Lett. **94**, 022102 (2009).
[20] P. Rinke, M. Scheiffler, A. Qteish, M. Winkelnkemper, Appl. Phys.Lett. **89**, 61919 (2006).
[21] M. Akarsu, S. Aydogu, O. Ozbas, Phys. Stat. Sol. (c) **4**(2), 664 (2007).
[22] S. Berrah, A. Boukortt, H. Abid, Phys. Scr. **75**, 414, (2007).
[23] V. M. Polyakov, F. Schewierz, Appl. Phys. Lett. **88**, 032101 (2006).

*Corresponding author: makarsu@ogu.edu.tr